Individual S-acylated cysteines differentially contribute to H-Ras endomembrane trafficking and acylation/deacylation cycles

Maria P. Pedro[a], Aldo A. Vilcaes[a], Guillermo A. Gomez[b], and Jose L. Daniotti[a,*]
[a]Centro de Investigaciones en Química Biológica de Córdoba, CIQUIBIC, CONICET, and Departamento de Química Biológica, Facultad de Ciencias Químicas, Universidad Nacional de Córdoba, Ciudad Universitaria, X5000HUA, Córdoba, Argentina; [b]Division of Cell Biology and Molecular Medicine, Institute for Molecular Bioscience, University of Queensland, St. Lucia, QLD 4072, Australia

ABSTRACT **S-acylation/deacylation cycles and vesicular transport are critical for an adequate subcellular distribution of S-acylated Ras proteins. H-Ras is dually acylated on cysteines 181 and 184, but it is unknown how these residues individually contribute to H-Ras trafficking. In this study, we characterized the acylation and deacylation rates and membrane trafficking of monoacylated H-Ras mutants to analyze their contributions to H-Ras plasma membrane and endomembrane distribution. We demonstrated that dually acylated H-Ras interacts with acyl-protein thioesterases (APTs) 1 and 2 at the plasma membrane. Moreover, single-acylation mutants of H-Ras differed not only in their subcellular distribution, where both proteins localized to different extents at both the Golgi complex and plasma membrane, but also in their deacylation rates, which we showed to be due to different sensitivities to APT1 and APT2. Fluorescence photobleaching and photoactivation experiments also revealed that 1) although S-acylated, single-acylation mutants are incorporated with different efficiencies into Golgi complex to plasma membrane vesicular carriers, and 2) the different deacylation rates of single-acylated H-Ras influence differentially its overall exchange between different compartments by nonvesicular transport. Taken together, our results show that individual S-acylation sites provide singular information about H-Ras subcellular distribution that is required for GTPase signaling.**

Monitoring Editor
Adam Linstedt
Carnegie Mellon University

Received: Aug 19, 2016
Revised: Jan 9, 2017
Accepted: Jan 30, 2017

INTRODUCTION

Ras family proteins are monomeric guanosine triphosphatases (GTPases) that couple extracellular signals to the intracellular effector pathways that control cell proliferation, differentiation, and survival (Wennerberg *et al.*, 2005). Dysregulation of these cellular functions is a hallmark of cancer, with activating mutations in Ras having been detected in ~20–35% of all human cancers (Ahearn *et al.*, 2012).

There are four ubiquitous (although functionally nonredundant; Hancock, 2003; Eisenberg *et al.*, 2013) Ras isoforms, namely H-Ras, N-Ras, K-Ras4A, and K-Ras4B. The source of this nonredundancy relies on the Ras C-terminus hypervariable region, which is <10% homologous between the different Ras isoforms and contributes differentially to their membrane-binding properties. Within this region, all Ras isoforms have a CAAX sequence (in which C is a cysteine, A is an aliphatic amino acid, and X is any amino acid) at the C-terminus that directs the posttranslational modification by farnesylation and methylation. These modifications convert an otherwise globular hydrophilic protein to one that associates with the cytoplasmic leaflet of cellular membranes (Wright and Philips, 2006; Ahearn *et al.*, 2012). Depending on the Ras isoform, a second signal for the membrane anchor is present in proximity to the farnesylation site and

This article was published online ahead of print in MBoC in Press (http://www.molbiolcell.org/cgi/doi/10.1091/mbc.E16-08-0603) on February 8, 2017.

*Address correspondence to: Jose Luis Daniotti (daniotti@fcq.unc.edu.ar).

Abbreviations used: 2-BP, 2-bromopalmitate; APT, acyl-protein thioesterase; FLIP, fluorescence loss in photobleaching; FRAP, fluorescence recovery after photobleaching; FRET, Förster resonance energy transfer; GTPase, guanosine triphosphatase; PAT, palmitoyltransferase; ROI, region of interest.

within the hypervariable region. In particular, H-Ras is posttranslationally S-acylated at cysteines 181 and 184, and N-Ras is S-acylated at cysteine 184, whereas K-Ras4B is not further modified with lipids but contains a polybasic domain with a binding capacity to anionic phospholipids. K-Ras4A is actually unique among the four Ras proteins in that it possesses a dual membrane-targeting motif of both an S-acylated cysteine and a polybasic region (Silvius *et al.*, 2006; Gomez and Daniotti, 2007; Cox *et al.*, 2015).

Beyond its role as a second signal for membrane binding, S-acylation is an important posttranslational modification on H-Ras, N-Ras and K-Ras4A isoforms, as it is the only lipid modification that is reversible by the action of palmitoyltransferases (PATs), which catalyze S-acylation, and also acyl-protein thioesterases (APTs), which catalyze S-deacylation. Moreover, the concerted action of PATs and APTs makes it possible for S-acylated proteins to undergo several cycles of acylation/deacylation during their lifetimes (Salaun *et al.*, 2010; Chamberlain and Shipston, 2015), which is critical for the adequate localization and trafficking of S-acylated Ras isoforms (Goodwin *et al.*, 2005; Rocks *et al.*, 2005; Tomatis *et al.*, 2010).

S-acylation of H-Ras in mammalian cells has been shown to depend on DHHC9/GCP16 palmitoyl transferase (Lobo *et al.*, 2002; Swarthout *et al.*, 2005), whereas the enzymes that catalyze its deacylation are APT1 and APT2, two cytosolic APTs that have been described to deacylate G_s α-subunit of trimeric G-proteins and H-Ras (Duncan and Gilman, 1998; Zeidman *et al.*, 2009; Tomatis *et al.*, 2010; Lin and Conibear, 2015b). More recently, ABHD17, a protein depalmitoylase, was also found to deacylate N-Ras, as well as postsynaptic density-95 protein (Lin and Conibear, 2015a; Yokoi *et al.*, 2016).

Cycles of acylation and deacylation are important in regulating the H-Ras function (Baines *et al.*, 2011; Verstraeten *et al.*, 2011), with perturbations in the acylation/deacylation machinery of H- and N-Ras not only affecting its subcellular distribution, but also partially reversing the phenotype of H-Ras–transformed epithelial cells and inhibiting the growth of N-Ras(G12D) mutant hematopoietic cells (Dekker *et al.*, 2010; Hedberg *et al.*, 2011; Xu *et al.*, 2012; Spiegel *et al.*, 2014). Of note, an in vivo RNA interference screen identified APT2 as a candidate regulator of oncogenic H-Ras–dependent malignancy (Beronja *et al.*, 2013).

In addition to being reversible, the attachment of fatty acid to H-Ras by S-acylation is required for H-Ras inclusion into vesicular carriers, which also contributes to the overall subcellular distribution of palmitoylated H-Ras. The dual acylation of H-Ras has been shown to be required for its endosomal transport and efficient plasma membrane localization (Gomez and Daniotti, 2005; Goodwin *et al.*, 2005; Rocks *et al.*, 2005), but mutation of acylation sites has caused H-Ras to accumulate in different subcellular compartments (Roy *et al.*, 2005).

In spite of these recent advances in the characterization of the biochemistry of S-acylation and H-Ras vesicular trafficking, it is still unclear whether single acylation sites contribute differentially to processes that lead to correct H-Ras subcellular localization and therefore its capacity to engage subcellular signaling. Here we demonstrate that S-acylated cysteines 181 and 184 contribute differentially to H-Ras membrane affinity and exhibit distinct APT sensitivities and deacylation kinetics. Furthermore, single acylated H-Ras undergoes (and to different extents) vesicular-mediated intracellular trafficking at the level of the post-Golgi complex, with the palmitoylated cysteine 184 more efficient at being incorporated into the Golgi to plasma membrane vesicular carriers. Of note, both single-acylated mutants exhibit deacylation-dependent and -independent diffusion with rapid reversible membrane binding to different intracellular organelles. Thus our results indicate that cysteines 181 and 184 provide unique information for spatial organization and trafficking of H-Ras, thereby influencing its steady-state subcellular distribution and capacity to activate downstream signaling.

RESULTS

H-Ras(C181S) and H-Ras(C184S) mutants are membrane associated, S-acylated, and able to engage Ras downstream signaling

To have a better understanding of how acylation/deacylation cycles on cysteines 181 and 184 contribute to the efficient subcellular distribution of H-Ras, we decided to characterize in detail the subcellular localization and acylation/deacylation processes of wild-type ($H\text{-}Ras^{WT}$), H-Ras(C181S), and H-Ras(C184S) single-acylation mutants and compared them to non–S-acylatable H-Ras(C181S,C184S) by using live-cell imaging (Figure 1A). As we reported previously (Gomez and Daniotti, 2005) for CHO-K1 cells, doubly acylated $H\text{-}Ras^{WT}$ was localized at the plasma membrane and recycling endosomes (colocalizing with endocytosed transferrin) and showed no colocalization with the Golgi complex markers GalNAc-T (*trans*-Golgi network [TGN]) and Sial-T2 (proximal Golgi complex; Figure 1Bi and Supplemental Figure S1). In contrast, single-acylation mutants of H-Ras revealed a different pattern of subcellular localization. H-Ras(C181S) was mostly present in Golgi membranes and only minimally localized at the plasma membrane, whereas H-Ras(C184S) was present at both the plasma membrane and the Golgi complex. However, neither was detected in recycling endosomes (Figure 1B, ii and iii, and Supplemental Figure S1). In contrast, nonacylated H-Ras(C181,184S) localization largely extended throughout the cell and was associated mainly with the endoplasmic reticulum and Golgi complex, as reported previously (Figure 1Biv; Choy *et al.*, 1999). These results agree with our previous investigation showing that dual acylation constitutes a sorting signal for recycling endosome localization (Trenchi *et al.*, 2009) and reveals critical differences in the role of single-acylation sites of H-Ras in its Golgi complex versus plasma membrane localization. A similar pattern of organelle distribution for H-Ras(C181S) and H-Ras(C184S) was observed in COS-7, HeLa, and NIH 3T3 cells (Supplemental Figure S2, A–C).

We then explored the possibility that the differences observed in subcellular distribution could be a consequence of alterations in membrane association and/or a posttranslational modification of H-Ras. To test this, we performed biochemical experiments to analyze the membrane binding and extent of lipidation of H-Ras when expressed in CHO-K1 cells. Our results demonstrated that H-Ras(WT), H-Ras(C181S), H-Ras(C184S), and H-Ras (C181S,C184S) were preferentially bound to cellular membranes, as these partitioned mostly to the pellet fraction after ultracentrifugation at 400,000 × *g* (Figure 1C). In addition, Triton X-114 partition assays of membrane and cytosolic fractions revealed that all of the H-Ras proteins were enriched in the detergent phase, which indicates the highly hydrophobic character of the protein conferred by farnesylation and/or S-acylation (Figure 1D; Gomez and Daniotti, 2005).

Because live-cell imaging experiments suggested that H-Ras(C181S) and H-Ras(C184S) behave differently from the nonacylatable H-Ras(C181,184S), these mutants might be posttranslationally S-acylated. To try to confirm this, we used two independent methods. First, we directly evaluated the S-acylation of these mutants (and $H\text{-}Ras^{WT}$ as control) by acyl biotinyl exchange (ABE) assays (Wan *et al.*, 2007), which demonstrated the acylation of the H-Ras(C181S) and H-Ras(C184S) versions (Figure 1E). Second, we performed a synchronized protein expression protocol (Trenchi *et al.*, 2009) in the presence of the S-acylation inhibitor 2-bromopalmitate (2-BP, 50 μM; Figure 1F) to impede the palmitoylation of newly

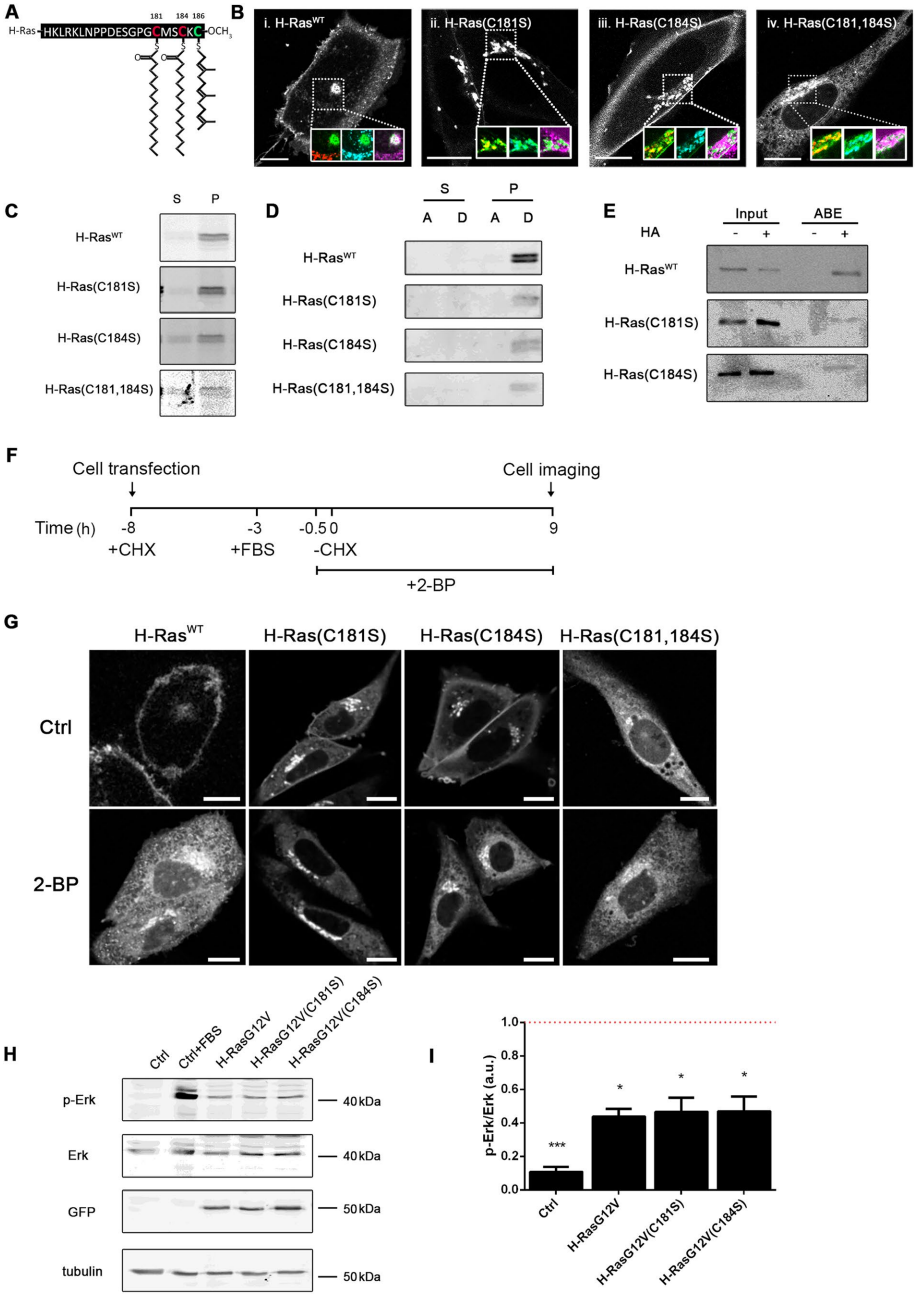

synthesized H-Ras. Under these conditions, blocking of S-acylation prevented the localization of H-Ras^{WT}, H-Ras(C181S), and H-Ras(C184S) at the plasma membrane and redistributed them to membranes of the endoplasmic reticulum and the Golgi complex, similarly to the observed distribution of nonacylatable H-Ras(C181,184S) (Figure 1G). As expected, 2-BP did not affect the subcellular localization of the double-cysteine mutant. These experiments confirm that H-Ras(C181S) and H-Ras(C184S) are S-acylated and suggest that the differences in subcellular distribution might be due to differential palmitate turnover.

Because our results showed that the dual acylation of H-Ras is not absolutely essential for the protein to remain membrane attached (Figure 1, B, D, and G), we then investigated whether mutation of single acylation sites would allow H-Ras still to be able

FIGURE 1: S-acylation, membrane association, and subcellular localization of H-Ras palmitoylation mutants. (A) Schematic representation of H-Ras C-terminal hypervariable region and its posttranslational modifications. (B) CHO-K1 cells were cotransfected with H-Ras^{WT}, H-Ras(C181S), H-Ras(C184S), or H-Ras(C181,184S) fused to YFP (pseudocolored green in the insets) and Golgi markers GalNAc-T-Cherry (pseudocolored red) and Sial-T2-CFP (pseudocolored cyan). Then they were incubated with Alexa Fluor 647–Tf (pseudocolored magenta) and analyzed by fluorescence confocal microscopy. Insets, zoomed images of the indicated region, as well as the colocalization with the organelle markers. Scale bars, 10 μm. (C) Subcellular fractionation. CHO-K1 cells transfected with H-Ras^{WT}, H-Ras(C181S), H-Ras(C184S), or H-Ras(C181,184S) fused to YFP were lysed and ultracentrifuged, and the supernatant (S) and pellet (P) fractions were separated. Proteins from these fractions were Western blotted with an antibody to GFP. (D) Triton X-114 partition assay. CHO-K1 cells transfected with H-Ras^{WT}, H-Ras(C181S), H-Ras(C184S), or H-Ras(C181,184S) fused to YFP were lysed and ultracentrifuged, and the supernatant (S) and pellet (P) fractions were separated. Then buffer containing 1% Triton X-114 was added, and phase separation was induced by incubation at 37°C. Proteins from aqueous (A) and detergent (D) phases were Western blotted with an antibody to GFP. (E) S-acylation detection by ABE assay. CHO-K1 cells transiently transfected with H-Ras^{WT}, H-Ras(C181S), or H-Ras(C184S) fused to YFP were lysed and incubated with NEM to block free thiols and treated or not with hydroxylamine (HA) to hydrolyze thioester bonds. After incubation with HPDP-biotin, biotinylated proteins were pulled down with streptavidin agarose beads and analyzed by Western blot using an antibody to GFP. Samples collected before (Input) and after (ABE) the pull down in conditions without (–HA) or with (+HA) hydroxylamine treatment. (F) Workflow of the experimental procedure used in G. CHO-K1 cells were transfected with H-Ras^{WT}, H-Ras(C181S), H-Ras(C184S), or H-Ras(C181,184S) fused to YFP in the presence of cycloheximide (CHX). At 30 min before CHX withdrawal, cells were incubated with 50 μM 2-BP or DMSO (vehicle, Ctrl). At 0 h, CHX was removed, and cells were further incubated with 2-BP or DMSO for 9 h. Finally, cells were analyzed by fluorescence confocal microscopy. (G) Representative images of H-Ras^{WT}, H-Ras(C181S), H-Ras(C184S), and H-Ras(C181,184S) fused to YFP, showing the effect of 50 μM 2-BP or DMSO (Ctrl) on subcellular distribution. Scale bars, 10 μm. (H) CHO-K1 cells nontransfected (Ctrl) or transfected with H-RasG12V, H-RasG12V (C181S), or H-RasG12V (C184S)-YFP were harvested in serum-free medium and analyzed by Western blot. A control condition was performed by incubating the cells with 10% FBS for 10 min to reveal the Erk1/2 activation (second line, Ctrl + FBS). The blots show the signal obtained by incubation with specific antibodies to phosphorylated Erk1/2 (p-Erk), total Erk (Erk), GFP, and tubulin. The blots are representative of three independent experiments. (I) Quantification of the experiment in H. Bars show mean amount of phosphorylated Erk relative to total Erk (arbitrary units [a.u.]) obtained in three independent experiments ± SEM. These values were relativized to the pErk/Erk of the Ctrl + FBS sample (shown as a dotted line). *$p < 0.05$; ***$p < 0.001$.

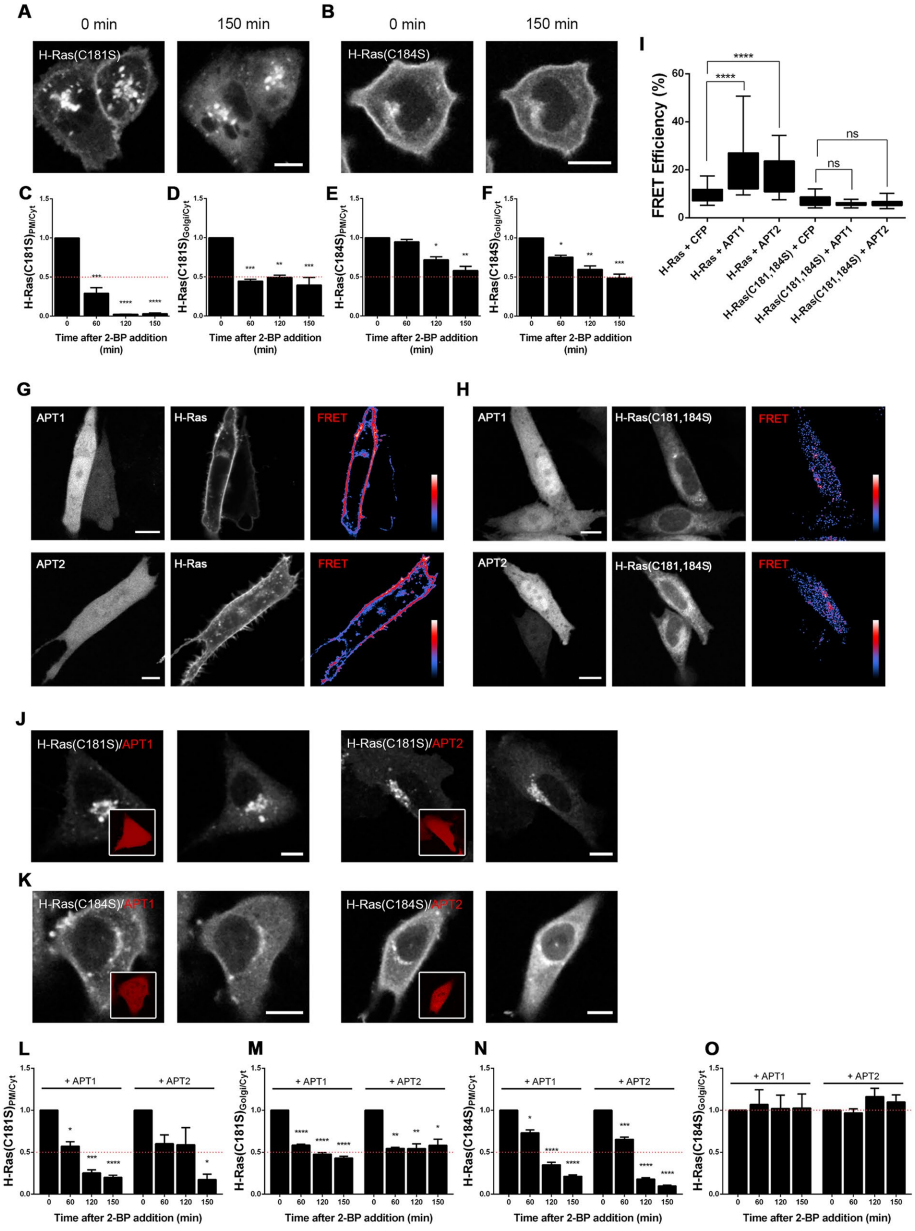

FIGURE 2: APT-driven deacylation of monoacylated versions of H-Ras in the plasma membrane and Golgi complex. (A, B) CHO-K1 cells were transfected to express H-Ras(C181S) or H-Ras(C184S)-YFP and analyzed by live-cell confocal fluorescence microscopy. At the beginning of the experiment, 50 μM 2-BP was added and maintained in the medium during all the procedure. Representative images taken at the start (0 min) and end (150 min) of each experiment. Scale bars, 10 μm. (C–F) Quantification of the obtained images (for details, see *Materials and Methods*). Bars represent the fluorescence in plasma membrane (PM) or Golgi complex relative to the cytoplasm fluorescence at different times after the addition of 2-BP. Data are expressed as mean ± SEM of two to six experiments performed independently. (G, H) CHO-K1 cells were cotransfected to express APT1-CFP or APT2-CFP (donor) and H-Ras^{WT} or H-Ras(C181,184S)-YFP (acceptor), and the FRET experiment was performed. FRET efficiency was evaluated by acceptor-sensitized emission (right). Representative cells undergoing FRET, with the respective scale of colors indicated in each FRET panel. Scale bars, 10 μm. (I) Quantification of FRET experiments in G and H. Values of FRET efficiency represented as percentages. H-Ras^{WT} + CFP and H-Ras(C181,184S) + CFP were used as negative controls. A representative experiment from three experiments performed independently. The number of cells analyzed in each case was ~40. (J, K) CHO-K1 cells were cotransfected to express H-Ras(C181S) or H-Ras(C184S)-YFP and APT1-CFP or APT2-CFP (pseudocolored red) and analyzed by live-cell confocal fluorescence microscopy. At the beginning of the experiment, 50 μM 2-BP was added and maintained in the medium during all the procedure. Representative images taken at the start (0 min) and end (120 min) of each experiment. Insets, expression of APTs. Scale bars, 10 μm. (L–O) Quantification of the images (for details, see *Materials and Methods*). Bars represent the fluorescence of each protein in plasma membrane (PM) or Golgi complex relative to the cytoplasm fluorescence at different times after the addition of 2-BP. Data are expressed as mean ± SEM of two to six experiments performed independently. ns, nonsignificant; *$p < 0.05$; **$p < 0.01$; ***$p < 0.001$; ****$p < 0.0001$.

to engage downstream signaling. To carry this out, we generated single-acylation mutants in a background of a constitutively active H-Ras mutant (H-RasG12V), a mutation largely known to impair intrinsic GAP-mediated GTPase function (Hobbs *et al.*, 2016). Transfected as well as control CHO-K1 cells were harvested in serum-free medium and then processed for Western blot analysis. We observed that there was no difference between the phosphorylation state of Erk1/2 in cells expressing dually acylated H-RasG12V or monoacylated H-RasG12V mutants (Figure 1, H and I). Of note, endomembrane distribution of the oncogenic versions of dually and monoacylated H-Ras was similar to the localization of their nonmutated counterparts (Supplemental Figure S3).

Taken together, the results show that H-Ras^{WT}, H-Ras(C181S), and H-Ras(C184S) exhibit different subcellular distributions, are S-acylated, and associate to membranes and activate Erk1/2 to the same extent. These agree with the notion that H-Ras signaling can proceed on endomembranes (Chiu *et al.*, 2002; Arozarena *et al.*, 2011; Agudo-Ibanez *et al.*, 2015).

Acyl-protein thioesterases deacylate H-Ras(C181S) and H-Ras(C184S) mutants with different kinetics at the plasma membrane

Having demonstrated that 1) differentially acylated versions of H-Ras have different subcellular localizations, 2) these differences depend on the incorporation and position of fatty acids, and 3) oncogenic versions of H-Ras acylation mutants are able to stimulate downstream effectors, we studied in more detail the deacylation process of these proteins. CHO-K1 cells transiently expressing H-Ras(C181S) or H-Ras(C184S) were incubated with cycloheximide for 1 h (to prevent protein synthesis) and then treated with 50 μM 2-BP to inhibit the PATs but not the thioesterases activities, as previously demonstrated for GAP-43 (Pedro *et al.*, 2013) and biochemically for H-Ras (Supplemental Figure S4). At the same time, we monitored H-Ras subcellular localization by live-cell imaging (Figure 2, A and B). We observed that H-Ras(C181S) fluorescence on the plasma membrane decayed significantly, with a

simultaneous increase in its cytoplasmic pool (probably endoplasmic reticulum) over time, suggesting that this pool of H-Ras mutant was completely deacylated within the time scale of our experiments (~120 min; Figure 2C). However, the most significant pool of this protein, localized at the Golgi complex, was still present, although affected by the addition of 2-BP (Figure 2D). A similar result was observed using cerulenin, a fungal inhibitor of PATs and hence of H-Ras (Lawrence *et al.*, 1999; Chen *et al.*, 2003; unpublished data). Regarding H-Ras(C184S), its plasma membrane and Golgi complex association clearly decreased throughout the experiment, indicating depalmitoylation activity (Figure 2, E and F). Nevertheless, this deacylation process seemed to be less efficient than that observed for the H-Ras(C181S) mutant in both subcellular localizations. These experiments were further complemented by analyzing the Manders overlap coefficient between H-Ras(C181S, C184S) and organelle markers (plasma membrane and Golgi complex markers) before and after 2-BP treatment (Supplemental Figure S5). As observed in Supplemental Figure S5, the degree of overlap between monoacylated H-Ras and the plasma membrane marker was drastically reduced after addition of 2-BP. In contrast, there was no significant change in pixel overlap at the Golgi complex at the beginning or end of incubation with the inhibitor, suggesting the presence of a mixed pool of H-Ras molecules (acylated and deacylated) in this compartment. The results indicate that deacylation at the Golgi complex might not be as efficient as at the plasma membrane for H-Ras(C181S) and that deacylation on the C181 and C184 residues is not biochemically and functionally equivalent, with deacylation on H-Ras(C181S) being more significant than for H-Ras(C184S).

One possible explanation for the different deacylation kinetics of H-Ras at the plasma membrane compared with endomembrane could be differential interaction between APTs and their substrates at these two subcellular locations in CHO-K1 cells. Although both APT1 and APT2 are able to deacylate Ras (Dekker *et al.*, 2010; Tomatis *et al.*, 2010), whether they interact differentially with H-Ras^{WT} and/or interact with it at different subcellular locations remain to be determined. Thus, to evaluate first the potential role of these proteins on H-Ras deacylation, we performed Förster resonance energy transfer (FRET) experiments to investigate the physical interaction between the cytosolic APTs and plasma membrane-associated H-Ras^{WT}. For FRET to occur, proteins attached to appropriate fluorophores must lie within 1–10 nm of each other for energy transfer to take place, which could be interpreted as a protein–protein interaction because this takes place on a similar spatial scale. Therefore we coexpressed H-Ras–yellow fluorescent protein (YFP) with either APT1–cyan fluorescent protein (CFP) or APT2-CFP in CHO-K1 cells, and, as negative control, we coexpressed H-Ras–YFP and cytosolic CFP. We found that both cytosolic thioesterases physically interacted with H-Ras^{WT}, principally at the plasma membrane, with some weak FRET signals observed on other intracellular compartments, such as recycling endosomes (Gomez and Daniotti, 2005), where H-Ras^{WT} localized at steady state (Figure 2, G and I). Of note, neither APT1 nor APT2 underwent FRET with the nonpalmitoylated mutant H-Ras(C181,184S) (Figure 2, G and I). These results are consistent with the idea that H-Ras is a substrate of APT1 and APT2 (Dekker *et al.*, 2010; Tomatis *et al.*, 2010). Moreover, these findings suggest that deacylation of H-Ras^{WT} occurs mainly at the plasma membrane and/or that a palmitoylated substrate is necessary for the APTs to interact with H-Ras.

Differences in deacylation kinetics at the same subcellular compartment (i.e., Golgi complex or plasma membrane) were also observed when we analyzed H-Ras(C181S) and H-Ras(C184S), which suggests that these mutants may exhibit different sensitivities to the action of APTs, as we previously found for single-acylation mutants of GAP-43 (Tomatis *et al.*, 2010). To test whether this is the case for H-Ras single-acylation mutants, we measured their desorption kinetics from the plasma membrane and Golgi complex of cells overexpressing APT1 or APT2 in the presence of 2-BP (Figure 2, J and K). First, we analyzed the deacylation kinetics of H-Ras(C181S) at the plasma membrane, where this protein was barely localized (Figure 2L). A loss of signal on this membrane was evident at the analyzed times, although there was no increase in the deacylation kinetics, due to the overexpression of the APTs (compare with results from Figure 2C). This could have been a consequence of the small amount of plasma membrane–bound H-Ras(C181S) associated with a relatively high level of endogenous APT2 activity. In addition, no significant changes in the deacylation rate of H-Ras(C181S) at the Golgi complex were observed in APT-overexpressing cells compared to cells treated with only 2-BP.

In contrast, we found that overexpression of APT1 or APT2 significantly increased the deacylation kinetics at the plasma membrane of H-Ras(C184S), with it being faster in cells that overexpressed the latter, thus suggesting a slight preference of APT2 for this substrate (Figure 2N). In this case, Golgi complex fluorescence did not significantly change over time (Figure 2O), whereas association of H-Ras(C184S) with membranes from the endoplasmic reticulum clearly increased, indicating a direct connection between this organelle and the plasma membrane or, eventually, via a rapid and transient passage through the Golgi complex, establishing an equilibrium with the endoplasmic reticulum pool. However, it cannot be discarded that H-Ras(C181S) and H-Ras(C184S) could also be substrates for other thioesterases.

Individual cysteine groups contribute differentially to the Golgi exiting of H-Ras

In addition to the differences in deacylation kinetics and sensitivity to APT-mediated deacylation, a key aspect in the behavior of H-Ras(C181S) and H-Ras(C184S) is their relative expression in the Golgi complex and plasma membrane compartments, which suggests that acylation on the cysteine residues C181 and C184 contributes differentially to the dynamics of Golgi entrance and/or exiting. An important observation in relation to this phenomenon is the effect of 2-BP on the subcellular distribution of H-Ras(C181S) and H-Ras(C184S) (Figure 2, D and F). Although deacylation of both proteins is evident under these conditions (with an increase in the endoplasmic reticulum pool being observed), the persistence of the proteins' Golgi fraction under these circumstances is different. In particular, the Golgi/cytoplasm ratio decreases faster over time for H-Ras(C181S) than for H-Ras(C184S) (Figure 2, D and F), suggesting that H-Ras(C181S) could be incorporated into the Golgi complex to plasma membrane vesicular carriers and/or detach from the Golgi membranes more efficiently. To test this quantitatively, we measured the dynamics of Golgi complex exiting of the single-acylated protein pool that localizes in this compartment by fluorescence loss in photobleaching (FLIP), as we previously described for diacylated proteins (Trenchi *et al.*, 2009). CHO-K1 cells were cotransfected to express H-Ras(C181S)- or H-Ras(C184S)-YFP, and GalNAc-T-Cherry was used as an internal control and Golgi complex marker; cells were treated with cycloheximide to inhibit protein synthesis. A small region of interest (ROI) at the plasma membrane was selected and bleached by irradiation every 2 min for 1 h, and the fluorescence belonging to the Golgi complex was quantified (Figure 3A). We observed an important decrease in the signal from the fluorescent H-Ras(C181S) and H-Ras(C184S) attached at the Golgi complex, which reflected the

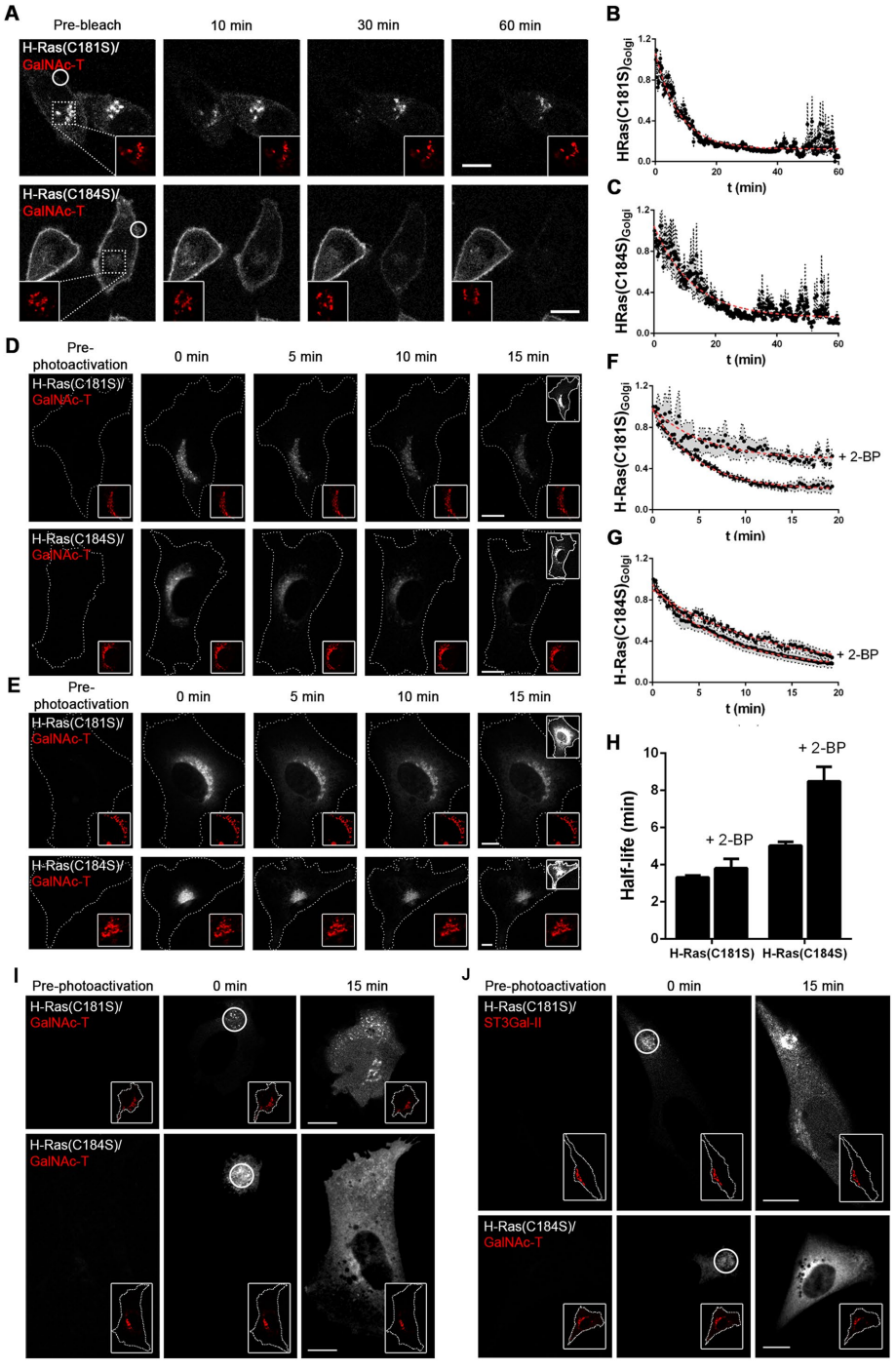

FIGURE 3: Traffic of monoacylated H-Ras versions from the Golgi complex. (A) FLIP experiment. CHO-K1 cells were cotransfected to express H-Ras(C181S) or H-Ras(C184S)-YFP and GalNAc-T-Cherry (Golgi complex marker, pseudocolored red) and treated with cycloheximide for 1 h before start of the experiment. Representative images at different times (prebleach and 10, 30, and 60 min). Repeated photobleaching was performed at the indicated area (white circle) every 2 min. Insets, zoomed images of the expression of GalNAc-T-Cherry in the indicated area. Scale bars, 10 μm. (B, C) Quantification of experiments in A. Golgi complex fluorescence was quantified as indicated in *Materials and Methods*. Data are expressed as mean ± SEM of three independent experiments. Red dotted line represents adjustment of the data to a one-phase decay equation. (D, E) Photoactivation at the Golgi complex. CHO-K1 cells were cotransfected to express H-Ras(C181S)-PAGFP or H-Ras(C184S)-PAGFP (pseudocolored gray) and GalNAc-T-Cherry (pseudocolored red). The area to photoactivate was chosen according to the expression of the Golgi marker. In the experiment with 2-BP (E), the inhibitor was added 15–30 min before start of image acquisition and maintained in the medium during the time of the experiment. Representative images at different times (prephotoactivation and 0, 5, 10, and 15 min). Bottom right, insets showing expression of GalNAc-T-Cherry over time. Top right, overexposed images to evidence the subcellular localization of fluorescence-activated H-Ras(C181S) or H-Ras(C184S). Scale bars, 10 μm. (F, G) Quantification of D and E, respectively. Golgi complex fluorescence was quantified as indicated in *Materials and Methods*. Data are expressed as mean ± SEM of three or four independent experiments. Red dotted line represents the adjustment of each data set to a one-phase decay equation. (H) Half-life of the protein at the Golgi complex calculated from F and G. (I, J) Photoactivation at the endoplasmic reticulum/cytosol. CHO-K1 cells were cotransfected to express H-Ras(C181S)-PAGFP or H-Ras(C184S)-PAGFP (pseudocolored gray) and GalNAc-T-Cherry (pseudocolored red) or ST3Gal-II-Cherry (pseudocolored red). The area to photoactivate is indicated with a white circle. In the experiment with 2-BP (J), the inhibitor was added 15–30 min before start of image acquisition and maintained in the medium during the time of the experiment. Cycloheximide was added 1 h before start of the experiment and maintained in the medium during the experiment. Repetitive photoactivation was performed in the selected area every 2 min. Representative images at different times (prephotoactivation and 0 and 15 min). Insets, expression of GalNAc-T-Cherry or ST3Gal-II-Cherry over time. Scale bars, 10 μm.

fact that proteins were being transported to the plasma membrane (Figure 3, B and C). However, this occurred with different dynamics for H-Ras(C181S): faster exit ($t_{1/2} = 5.5 \pm 0.2$ min) was noted than for H-Ras(C184S) ($t_{1/2} = 8.7 \pm 0.4$ min). This result is in agreement with our hypothesis that acylation of these residues contributes differentially to the dynamics of H-Ras trafficking.

To confirm these observations, we measured the residence time of H-Ras mutants at the Golgi complex in photoactivation experiments by analyzing the half-life of fluorescence decay of photoactivated H-Ras(C181S) and H-Ras(C184S) fused to photoactivable green fluorescent protein (PA-GFP; Patterson and Lippincott-Schwartz, 2004; Rocks *et al.*, 2005). Photoactivation experiments allow the residence time to be measured of a "snapshot pool" of H-Ras present at the Golgi complex. In the case of Ras proteins, this snapshot could be nonacylated or acylated proteins, and thus the kinetics of decay will reflect the residence half-life of these different protein populations. Our results showed that photoactivation of H-Ras(C181S) at the Golgi complex resulted

in a rapid decrease of fluorescence in this organelle, with a half-life of 3.3 ± 0.1 min and reaching up to a 20% of the initial value (Figure 3, D, F, and H). Its association with discrete structures (vesicles; Supplemental Movie S1) can also be observed, suggesting that the fluorescence at the Golgi complex was decaying because photoactivated molecules were incorporated efficiently into the vesicular carriers. Of interest, when this experiment was carried out in the presence of 2-BP, which led to efficient depalmitoylation of this mutant, there was a significant reduction in the exiting of H-Ras(C181S), with a half-life of 3.8 ± 0.5 min and a plateau value of 50% of the initial fluorescence (Figure 2, E, F, and H). Moreover, we did not observe the incorporation of depalmitoylated H-Ras into vesicular carriers under these conditions (Supplemental Movie S1). In fact, we noted that photoactivated H-Ras(C181S) began to appear in regions that belonged to the endoplasmic reticulum near the Golgi complex before rapidly diffusing throughout the entire organelle (see the overexposed box in Figure 3E). This suggests that although H-Ras(C181S) requires palmitoylation for its incorporation into carriers before Golgi complex exiting, this is not a requirement for Golgi exchange with the endoplasmic reticulum. A similar behavior was previously described for the diacylated, GABA-synthesizing enzyme GAD65 (Kanaani *et al.*, 2008). This strengthens the concept that under 2-BP treatment, the Golgi pool of H-Ras(C181S) is mostly nonacylated and that this pool of protein can rapidly redistribute (mainly to the endoplasmic reticulum) when photoactivated at the Golgi complex (Rocks *et al.*, 2010).

A different behavior was observed for H-Ras(C184S) when we analyzed the kinetics of fluorescence decay after photoactivation at the Golgi complex. With respect to H-Ras(C181S), a vesicular exit from this organelle was also evidenced for H-Ras(C184S), although with significantly slower kinetics ($t_{1/2} = 5.0 \pm 0.2$ min), which agreed with our previous FLIP results (Figure 3, D, G, and H, and Supplemental Movie S2). However, in the presence of 2-BP, the mobile fraction was not significantly different (as occurred the case of H-Ras(C181S)), but with significantly slower half-life (Figure 3E and Supplemental Movie S2). Given the fact that at steady state, H-Ras(C184S) is palmitoylated (Figure 1E) but with slower deacylation kinetics than H-Ras(C181S), this suggests that the percentages of acylated H-Ras (C184S) under control and 2-BP conditions are not dramatically different, and therefore similar decay curves should be expected as we observed in our experiments. Note that the decay rate was slower for H-Ras(C184S), indicating that the efficiency at which this is incorporated into vesicular carriers is lower than that of H-Ras(C181S). Finally, a repetitive photoactivation of H-Ras(C181S) and H-Ras(C184S) outside the Golgi complex (in a region that corresponded to the endoplasmic reticulum and cytosol) resulted in an accumulation of the proteins in this organelle, even in the presence of 2-BP (Figure 3, I and J). These results support the observation that a rapid and dynamic exchange exists between the endoplasmic reticulum and Golgi complex and that this exchange is independent of S-acylation.

Deacylation on individual cysteine groups contributes differentially to the Golgi pool of H-Ras

Our previous results showed that H-Ras single-acylated mutants are deacylated at the plasma membrane and travel from the Golgi complex to the plasma membrane and/or endoplasmic reticulum with differential kinetics and through different trafficking processes. Next we studied the retrograde transport by testing whether deacylation at the plasma membrane contributes directly to the Golgi complex pool, as observed for these proteins at steady state. To carry this out, we performed fluorescence recovery after photobleaching (FRAP) of the pool of the monoacylated H-Ras proteins associated to the Golgi complex. CHO-K1 cells were cotransfected to express the Golgi marker GalNAc-T-Cherry with H-Ras(C181S)- or H-Ras(C184S)-YFP and treated with cycloheximide to inhibit protein synthesis. Then the Golgi complex was photobleached by confocal laser microscopy and the region monitored for fluorescence recovery for 15 min. As shown in Figure 4A, H-Ras(C181S) was highly concentrated at the Golgi complex, colocalizing with GalNAc-T. After focal irradiation, the fluorescence was considerably reduced and began to rapidly reappear at this location (Figure 4A, top). Quantification of this event showed that the fluorescence recovered with a half-life ($t_{1/2}$) of 3.2 ± 0.4 min and a mobile fraction of 18%. Furthermore, fluorescence recovery on the Golgi complex seemed not to depend on PAT activity, because the pharmacological treatment of the cell with 50 μM 2-BP resulted in a fluorescence recovery with $t_{1/2} = 5 \pm 1$ min (Figure 4B), with no significant changes in the mobile fraction, in contrast to that observed for diacylated H-Ras in Madin–Darby canine kidney cells (Rocks *et al.*, 2005). This result suggests that H-Ras(C181S) was able to exchange with pools of the protein located elsewhere in the cell and that the observed Golgi complex pool of this protein did not necessarily reflect a pool that was being acylated by PATs, which concurs with our observation that nonpalmitoylated, photoactivated H-Ras(C181S) can be exchanged between the Golgi and endoplasmic reticulum. In contrast, FRAP experiments with H-Ras(C184S) resulted in a recovery of the fluorescence at the Golgi complex with $t_{1/2} = 3.5 \pm 0.7$ min (Figure 4A, bottom) and a 17% mobile fraction. In the presence of 2-BP, we observed that the recovery occurred with $t_{1/2} = 2.8 \pm 0.5$ min but with a significantly increased mobile fraction (~50% of the initial; Figure 4C), suggesting that under these conditions, deacylated H-Ras contributed more to the recovery rates observed.

Cycloheximide inhibits the FK506-binding protein (FKBP) family of prolyl isomerases (Christner *et al.*, 1999). FKBP12, a member of the FKBP family, binds to H-Ras in a palmitoylation-dependent manner and promotes depalmitoylation in a manner dependent on proline 179 (Ahearn *et al.*, 2011). In particular, FKBP12 only binds diacylated H-Ras, and association with nonpalmitoylated or monopalmitoylated H-Ras (C181S and C184S) was drastically reduced or inhibited, indicating that cycloheximide might not affect deacylation of these acylation mutants. Nonetheless, and considering that cycloheximide was used in our studies to inhibit protein synthesis, we performed controls by FRAP experiments in the presence of puromycin, which is a translation inhibitor lacking prolyl isomerase inhibitor activity (Ahearn *et al.*, 2011). As seen in Supplemental Figure S6, the kinetics of photobleaching recovery of H-Ras(C181S) and H-Ras(C184S) at the Golgi complex were similar in the presence of cycloheximide and puromycin, denying a modulatory effect of FKBP12 on the trafficking of these monoacylated mutants.

Next we sought to investigate the contribution of the plasma membrane pool of H-Ras to the fluorescence recovery at the Golgi complex. FRAP experiments were performed in the presence of tannic acid, a nonpermeable mild fixative that functionally impairs the plasma membrane without affecting the trafficking between the organelles of the rest of the endomembrane system (Polishchuk *et al.*, 2004; Paladino *et al.*, 2006; Trenchi *et al.*, 2009). Under these conditions, the fluorescence recovery at the Golgi complex was inhibited for both monoacylated mutants of H-Ras (Figure 4, B and C), demonstrating that a significant fraction of the proteins again reached the Golgi complex, probably through exchange with the plasma membrane. Moreover, when FRAP experiments were performed for H-Ras(C184S) in the presence of tannic acid and 2-BP, fixation at the plasma membrane blocked the increase in the mobile fraction caused by 2-BP, revealing again that deacylation at the plasma membrane contributed to the steady-state Golgi pool of H-Ras(C184S). In addition, because

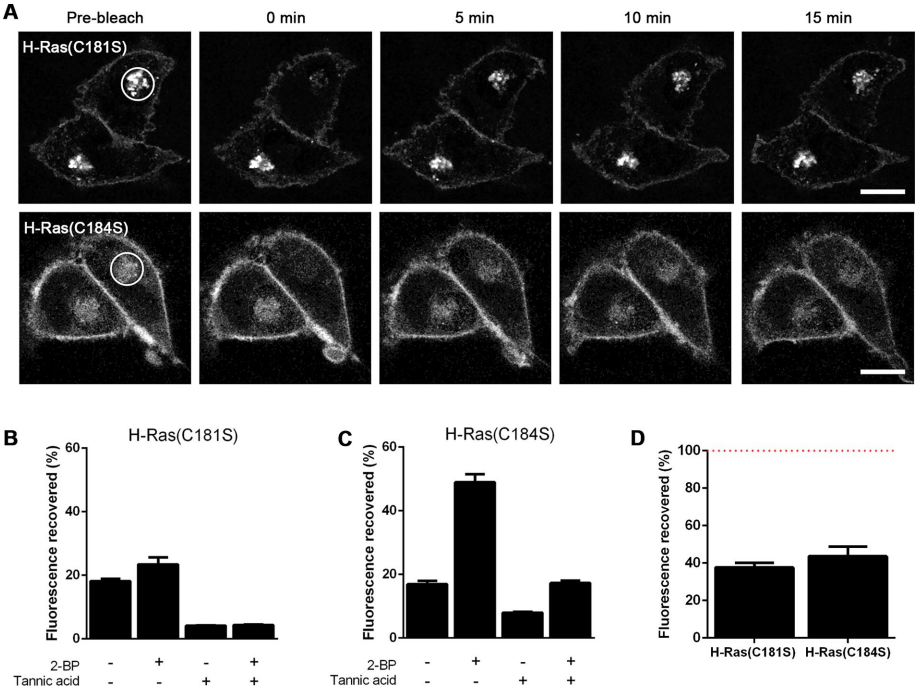

FIGURE 4: Traffic of monoacylated H-Ras versions to the Golgi complex. (A) FRAP experiment. CHO-K1 cells were cotransfected to express H-Ras(C181S) or H-Ras(C184S)-YFP and the Golgi marker GalNAc-T-Cherry (not shown) and treated with cycloheximide for 1 h before start of the experiment. Representative images at different times (prebleach and 0, 5, 10, and 15 min). The area photobleached is indicated by a white circle. Images were taken every 30 s for 15 min after photobleaching. Scale bars, 10 μm. (B, C) FRAP experiments were performed in the presence of 2-BP and tannic acid. In the experiments with 2-BP, the inhibitor was added 15 min before start of image acquisition and maintained in the medium during the time of the experiment. Tannic acid was added when indicated to a final concentration of 1%. The photobleached area colocalizes with the Golgi marker, and images were taken every 30 s for 15 min after the photobleaching. Golgi complex fluorescence was quantified as indicated in *Materials and Methods*. Bars plots show the amount of Golgi fluorescence at the end of the experiment for three to six experiments performed independently. (D) FRAP experiments were performed in the presence of the β-lactone APT inhibitor palmostatin B. CHO-K1 cells were cotransfected to express H-Ras(C181S) or H-Ras(C184S)-YFP and the Golgi marker GalNAc-T-Cherry and treated with 10 μM palmostatin B for 15 min before start of the image acquisition and maintained in the medium during the time of the experiment. The photobleached area colocalizes with the Golgi marker, and images were taken every 15 s during 15 min after the photobleaching. Golgi complex fluorescence was quantified as indicated in *Materials and Methods*. Bars plots show the amount of Golgi fluorescence at the end of the experiment for six experiments performed independently. The values are expressed as a percentage of the control experiment (without palmostatin B, taken as 100% and showed as a dotted line).

tannic acid also perturbs endocytic trafficking, vesicular transport of monoacylated H-Ras mutants between the plasma membrane and the Golgi complex could also be contributing.

Finally, we performed experiments using the inhibitor palmostatin B, a β-lactone that forms a covalent complex with APT1, APT2, and other serine hydrolases (Dekker *et al.*, 2010; Rusch *et al.*, 2011; Lin and Conibear, 2015a). The presence of the thioesterase inhibitor clearly decreased the rate of retrieval of monoacylated H-Ras from plasma membrane to Golgi complex, as monitored by FRAP experiments (Figure 4D). Thus the results reinforce the notion that both deacylation at the plasma membrane and a vesicular transport are primary processes for Golgi complex trafficking.

DISCUSSION

According to the classical signal transduction models, stimulation of growth factor receptors at the cell surface leads to the activation and accumulation of components in the inner leaflet of the plasma membrane, which in turn results in the generation of second messengers or activation of specific target proteins (Di Fiore and Gill, 1999). Under this scenario, endocytosis was previously considered to be involved in the termination of a signal by removing the receptor from the cell surface and promoting uncoupling of the ligand–receptor complex. In recent years, this paradigm has changed completely because of new evidence linking endocytosis and trafficking to the regulation of signal transduction. Indeed, complete signal transduction platforms (i.e., Ras, Raf-1, phosphorylated MEK, and phosphorylated mitogen-activated protein kinase) were found to be associated with endocytic transport vesicles and endosomes after stimulation with epidermal growth factor and insulin (Pol *et al.*, 1998; Rizzo *et al.*, 2000, 2001; Jiang and Sorkin, 2002). However, the cellular and molecular mechanisms that govern intracellular distribution of many signaling molecules are still not well understood.

In the case of H-Ras, a dynamic turnover of palmitate was found to regulate the intracellular trafficking of this protein to and from the Golgi complex by shifting between nonvesicular and vesicular modes of transport (Goodwin *et al.*, 2005; Rocks *et al.*, 2005). We also provided evidence that H-Ras is endocytosed and delivered to the endocytic recycling compartment in Rab5- and Rab11-dependent vesicular transport (Gomez and Daniotti, 2005). However, due to the lack of a complete effect of GDP-bound Rab mutants on the internalization of H-Ras, we hypothesized that a small GTPase could be internalized using alternative and simultaneous pathways in which the rate of acylation/deacylation might regulate these processes. In the present study, we focused on APT-driven deacylation of differentially acylated species of H-Ras and how it could affect the dynamic and intracellular trafficking of this GTPase.

Although experiments performed on different cell lines indicated that H-Ras S-acylation is not absolutely essential for the protein to remain membrane attached, it is a necessary condition for endomembrane localization. In fact, both the stoichiometry and the position of fatty acids in H-Ras had a great influence on the cell type–dependent distribution. In particular, we found that these sites exhibit a differential preference for APTs and for incorporation into vesicular carriers. This confirms a previous hypothesis that hydrophobicity of the fatty acid and prenyl groups, as well as the spacing between them, is relevant for Ras membrane association and trafficking (Roy *et al.*, 2005). Supporting these observations, a theoretical study showed that cysteine 181-palmitate and cysteine 186-farnesyl alone provide a sufficient hydrophobic force for tight membrane binding of H-Ras, whereas palmitoyl at cysteine 184 does not provide extra affinity but contributes to lateral membrane segregation (Gorfe and McCammon, 2008), which in cells might affect its incorporation into vesicular carriers. Nevertheless, despite their different subcellular

localizations, the oncogenic active mutants (G12V) of H-Ras, H-Ras(C181S), and H-Ras(C184S) were capable of activating Erk1/2 to the same extent. From these findings, we speculated that transient binding to membranes (not readily visible in fixed samples) could be a full requirement for wild-type and oncogenic versions of H-Ras acylation mutants (although mostly mislocalized) to become activated and interact with effectors.

As mentioned earlier, cysteines 181 and 184 also showed different susceptibilities to the action of APTs, in particular at the plasma membrane. Time-lapse in vivo experiments revealed that in cells treated with the S-acylation inhibitor (2-BP) or up-expressing APT1 or APT2, the plasma membrane and Golgi complex pools of H-Ras have acylation/deacylation cycles with different dynamics associated with a fraction of nonpalmitoylated H-Ras attached to the Golgi complex. Furthermore, monoacylated H-Ras showed a faster deacylation dynamic than double-palmitoylated H-Ras (unpublished data; Tomatis *et al.*, 2010), similar to our results for monoacylated and diacylated GAP-43 (Pedro *et al.*, 2013). Our findings also revealed that APTs exhibit some degree of preference for substrates localized in different subcellular compartments. For H-Ras(C181S), which mainly accumulates at the Golgi complex, the fluorescence at this location is reduced over time, although with no significant differences among cells up-expressing APT1 or APT2 and the control condition. This concurs with the fact that APTs interact with acylated Ras only at the plasma membrane and/or that the majority of this protein is in a deacylated state at the Golgi complex. Similarly, no differences in the deacylation of H-Ras(C181S) were observed at the plasma membrane as a result of the overexpression of the APTs, suggesting a saturation of endogenous APT2 enzyme activity for this substrate. In contrast, APT1 or APT2 overexpression increased the deacylation kinetics at the plasma membrane of H-Ras(C184S), which was faster in cells expressing the latter, which suggests a slight preference of APT2 for this substrate. In any case, additional in vivo and in vitro biochemical experiments might be carried out to further support the differential activities of APTs against one or another S-acylated cysteine of H-Ras.

Because the extent of localization at the Golgi complex was different for the two monoacylated H-Ras proteins, we also characterized the dynamics of association of these proteins with membranes of this organelle. In the case of H-Ras(C181S), the association with the membrane from the Golgi complex seems not to depend on PAT activity because pharmacological treatment of the cell with the inhibitor 2-BP did not significantly modify FRAP. In contrast, the presence of S-acylation inhibitor increased both the half-time of fluorescence recovery and the mobile fraction of H-Ras(C184S), which may be explained by a larger pool of deacylated H-Ras(C184S) originating at the plasma membrane and arriving by diffusion to the Golgi complex. We also observed that the plasma membrane and Golgi complex pools of monoacylated H-Ras are connected and exchangeable and that both vesicular and diffusion transport are specifically involved in the retrograde journey of monoacylated H-Ras mutants. In particular, impairment of plasma membrane fusion and internalization by treatment with tannic acid does affect the trafficking of H-Ras(C181S) and H-Ras(C184S) from plasma membrane to the Golgi complex, which reveals a vesicle-mediated retrograde trafficking. Similarly, vesicular transport was previously demonstrated in the trafficking of dually palmitoylated GAP-43 and wild-type H-Ras from plasma membrane to the recycling endosomes in CHO-K1 cells (Gomez and Daniotti, 2005; Trenchi *et al.*, 2009). Further, when experiments were carried out in the presence of a thioesterases inhibitor, there was a marked reduction of fluorescence recovered at the Golgi complex, demonstrating the importance and contribution of the deacylation process in retrograde trafficking of monoacylated H-Ras mutants.

Taken together, our results show that the interplay between PAT and APT activities, as well as protein stability, can result in a heterogeneous distribution of acylated species whose physiological or pathological implications have been underestimated and poorly studied mainly due to technical limitations that make it difficult to obtain information on the fractional or total amount of protein that is fully or partially S-acylated. The first and only antecedent in this regard was reported by Resh and coworkers, who demonstrated by mass spectrometry that about one-third of the total GAP-43 population is monoacylated or dually S-acylated at the steady state in vivo (Liang *et al.*, 2002). More recently, mathematical modeling combined with experimental determinations predicted that calnexin, a potentially diacylated type I transmembrane protein, is either fully acylated or not acylated, whereas single-acylated species do not become significantly populated, due to a high rate of depalmitoylation (Dallavilla *et al.*, 2016). This might also be the case for H-Ras because a biochemical approach has recently shown the coexistence of this diacylated and nonacylated protein in neurons, whereas the monopalmitoylated species do not seem to be present in the analyzed cells (Yokoi *et al.*, 2016). Nevertheless, we hypothesize that single-acylated H-Ras must exist, at least transiently, when nascent Ras is being modified. Given that our data now show that single-acylation sites have different deacylation kinetics and exhibit different efficiencies of incorporation into appropriate vesicular carriers, we expect that incorporating this information into new numerical models will help to obtain a better understanding of the subcellular distribution of dually acylated H-Ras.

Summing up, our results indicate that each fatty acid moiety provides singular information for the spatial organization of H-Ras and suggest differential accessibility of fatty acids to APTs. Thus modulation of thioesterase activity in a particular cellular context, both physiological and pathological, could be relevant to orchestrate the type and dynamics of the intracellular transport of acylated isoforms of H-Ras (see the proposed trafficking model in Figure 5) and, as a consequence, influence the correct connection of the small GTPase with downstream signaling molecules. As mentioned earlier, the functional implication of differentially acylated H-Ras has been underestimated and poorly explored, but in light of our results, their transient or more permanent presence in different cellular contexts, associated with their dynamism and capacity to activate downstream effectors, should definitively be taken into consideration when studying the biology of H-Ras or developing anticancer therapies.

MATERIALS AND METHODS

Plasmids

The expression vectors pECFP-C1 (ECFP is enhanced CFP), pEYFP-C1 (EYFP is enhanced YFP), and pmCherry-C1 were obtained from Clontech. Expression plasmids for H-Ras-YFP, ^{N27}GalNAc-T-Cherry, Sial-T2-CFP, APT1-CFP, APT1-Cherry, APT2-CFP, APT2-Cherry, and ST3Gal-II-Cherry were previously described (Giraudo *et al.*, 1999; Gomez and Daniotti, 2005; Trenchi *et al.*, 2009; Tomatis *et al.*, 2010; Pedro *et al.*, 2013; Ruggiero *et al.*, 2015). Monoacylated and nonacylated mutants, as well as constitutively active H-RasG12V proteins, were constructed by PCR using H-Ras as a template and the appropriate primers.

Cell culture and DNA transfection

CHO-K1 cells (American Type Culture Collection, Manassas, VA) were maintained at 37°C and 5% CO_2 in DMEM supplemented with

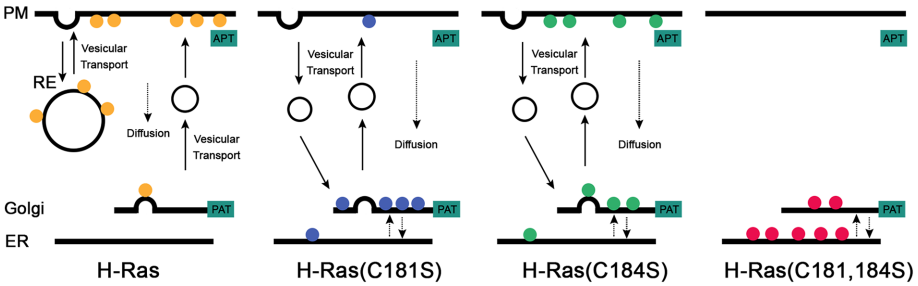

FIGURE 5: Subcellular trafficking model for acylated versions of H-Ras. The proposed model was designed taking into consideration information from the present and previous studies from different laboratories. H-Ras proteins are first modified in the cytosol with a farnesyl anchor to the cysteine 186 in the CAAX motif. After association with the cytosolic surface of the endoplasmic reticulum (ER), H-Ras arrives at the Golgi complex, where specific PAT S-acylates the cysteines 181 and 184. After dual acylation at the Golgi complex, H-Ras is included into the vesicular carriers directed to the plasma membrane (PM). At the cell surface, H-Ras is endocytosed, transported to recycling endosomes (RE), and recycled back to plasma membrane. A fraction of H-Ras could eventually be deacylated by APTs, returning by nonvesicular transport (Diffusion) to the Golgi complex and/or endoplasmic reticulum, where it is again acylated. H-Ras bearing only an acyl group at cysteine 184 (H-Ras(C181S)) or at cysteine 181 (H-Ras(C184S)) is mainly associated to the Golgi complex or the Golgi and plasma membrane, respectively. The endomembrane pools of monoacylated H-Ras are highly dynamic, connected, and exchangeable by vesicular transport and/or diffusion after APT deacylation. Consequently modulation of thioesterase activities is relevant to determine the mechanisms involved in the intracellular trafficking of acylated isoforms of Ras. Nonacylated and farnesylated H-Ras(C181,184S) was found at the Golgi complex in reversible connection with membranes of the endoplasmic reticulum.

10% fetal bovine serum (FBS) and antibiotics (100 µg/ml penicillin and 100 µg/ml streptomycin). Cells grown on Petri dishes were used for both live-cell imaging and Western blot experiments. These cells were transfected with 0.2–1 µg/35-mm dish of the indicated plasmid using cationic liposomes (Lipofectamine; Invitrogen) or polyethylenimine linear (Polysciences, Warrington, PA). At 24 h after cell transfection, cells were processed for Western blot experiments or plated onto Lab-Tek chambered coverglasses (Thermo Scientific Nunc), incubated for 24 h, and then used in live-cell imaging.

Subcellular fractionation and Triton X-114 partition assay

Subcellular fractionation, the Triton X-114 partition assay, electrophoresis, and Western blotting were performed as described (Crespo *et al.*, 2002; Gomez and Daniotti, 2005, 2007; Trenchi *et al.*, 2009) with some modifications. Cells grown onto 60-mm dishes were washed with cold phosphate-buffered saline (PBS; 140 mM NaCl, 8.4 mM Na_2HPO_4, 1.6 mM NaH_2PO_4, pH 7.5) and harvested by scraping in PBS containing protease inhibitors. Extracts were centrifuged at 4°C for 5 min at 13,000 × *g* and resuspended in 400 µl of 5 mM Tris-HCl (pH 7.0) in the presence of protease inhibitors. Pellets were dispersed by repetitive pipetting and vortexing. After 30 min of incubation, pellets were passed 60 times through a 25-gauge needle. Nuclear fractions and unbroken cells were removed by centrifuging twice at 4°C for 5 min at 600 × *g*. Supernatants were then ultracentrifuged at 4°C for 1 h at 400,000 × *g* using a TLA 100.3 rotor (Beckman Coulter). The supernatant (S1 fraction) was removed, and the pellet (P1 fraction) was resuspended in 400 µl of 5 mM Tris-HCl (pH 7.0). Both fractions were further ultracentrifuged at 400,000 × *g*, the supernatant of S1 fraction was removed (S fraction), and the pellet of P1 fraction was resuspended in 400 µl of buffer (P fraction). A 100-µl amount of 5% (vol/vol) TX-114 was added to the S and P fractions and incubated at 4°C for 1 h. Then samples were incubated at 37°C for 3 min and centrifuged at 13,000 × *g*. The aqueous upper phase (A) and the detergent-enriched lower phase (D) were separated and extracted again with detergent and aqueous solutions, respectively. The resulting samples were adjusted to equal volumes, and the detergent content and proteins were precipitated with chloroform:methanol (1:4 vol/vol) for electrophoresis and Western blot analyses.

Acyl biotinyl exchange

The ABE assay was carried out as reported in Wan *et al.* (2007) with some modifications. Briefly, transfected CHO-K1 cells grown in 100-mm dishes were washed with cold PBS, harvested, lysed, and centrifuged as described in the preceding subsection. Supernatant was removed, and Triton X-100 was added to a final concentration of 1.7% and incubated with end-over-end rotation at 4°C for 1 h. The proteins were precipitated with chloroform/methanol (1:4 vol/vol) and resuspended in SB (4% SDS, 50 mM Tris HCl, pH 7.4, 5 mM EDTA) with 10 mM *N*-ethylmaleimide (NEM) before incubation at 37°C with agitation. LB (50 mM Tris HCl, pH 7.4, 5 mM EDTA, 150 mM NaCl) with 1 mM NEM, 0.2% Triton X-100, protease inhibitor mix (PIM), and phenylmethylsulfonyl fluoride (PMSF) was added to each sample and incubated overnight at 4°C. NEM from samples was removed by three sequential chloroform/methanol precipitations, and they were finally resuspended in SB. The samples were divided into two equal portions, with one being incubated with HB (1 M hydroxylamine, pH 7.4, 150 mM NaCl, 0.2% Triton X-100, PIM, PMSF, 1 mM HPDP-biotin) and the other with TB (LB, 0.2% Triton X-100, PIM, PMSF, 1 mM HPDP-biotin) to use as a control at room temperature for 1 h. Then the proteins were precipitated with chloroform/methanol to remove unreacted HPDP-biotin and incubated with streptavidin agarose beads after resuspension. The samples were left 1 h at room temperature with end-over-end rotation. Then the elution was carried out in a buffer containing dithiothreitol. All samples were processed for Western blot analysis.

Endocytosis of Alexa Fluor 647–conjugated transferrin

This assay was performed as described in Iglesias-Bartolome *et al.* (2006).

Confocal microscopy and image acquisition

Confocal images were collected using an Olympus FluoView FV1000 confocal microscope (Olympus Latin America, Miami, FL) equipped with a multiline argon laser (458, 488, and 514 nm) and two helium–neon lasers (543 and 633 nm, respectively). CFP was detected by using laser excitation at 458 nm, a 458/514-nm excitation dichroic mirror, and a 470- to 500-nm band-pass emission filter. YFP was acquired by using laser excitation at 514 nm, a 458/514-nm excitation dichroic mirror, and a 530/570-nm band-pass emission filter. Cherry protein was acquired with a laser excitation at 543 nm, a 458/543/633-nm excitation dichroic mirror, and a 560-nm long-pass emission filter. Alexa Fluor 647 was acquired with a laser excitation at 633 nm, a 488/543/633-nm excitation dichroic mirror, and a 650-nm long-pass emission filter. For CFP/YFP/Cherry acquisition, images were sequentially acquired in line mode. This minimizes the bleedthrough between

channels mainly due to overlapping emission spectra of these fluorochromes.

Live-cell experiments were performed at 37°C (temperature and CO_2 controller; Tokai Hit, Japan) on an Olympus FluoView FV1000 confocal microscope.

For subcellular distribution analyses and colocalization of H-Ras and its acylation mutants with organelle markers, live-cell experiments were performed at 37°C using a 63×/1.42 numerical aperture (NA) Plan Apo objective oil immersion (Olympus, Japan). Images were taken using a 3× digital zoom and an appropriated pinhole to obtain 1 Airy unit for the fluorochrome of shortest wavelength excitation/emission properties (optical slice, 0.8 μm). Images of different cells for each dish were taken over a period no longer than 30 min. Images are representative of at least three independent experiments.

For deacylation measurements, cells coexpressing H-Ras–YFP or its acylation mutants and ^{N27}GalNAcT-Cherry or H-Ras–YFP, ^{N27}GalNAcT-Cherry, and APT1/2-CFP were treated with cycloheximide 1 h before start of the experiments. Live-cell experiments were performed at 20°C on the Olympus FluoView FV1000 confocal microscope to minimize vesicular trafficking (Tomatis *et al.*, 2010) and in the presence of 50 μM 2-BP to inhibit PAT but not APT activity (Pedro *et al.*, 2013). After selection of cells coexpressing all proteins, images were acquired in the YFP and Cherry channels for deacylation kinetic measurements using a 63×/1.42 NA Plan Apo oil immersion objective (Olympus) with a 3× digital zoom. The image resolution was 512 × 512 pixels, with a scan speed of 10 ms/pixel, and the pinhole was adjusted to obtain an optical slice of 3 μm. Single two-dimensional images were taken at a frequency of 5 min^{-1} for 150 min. These acquisition conditions were optimized to minimize bleaching and to sample as rapidly as possible the amount of H-Ras at the plasma membrane. All image analysis and the quantification method were carried out using ImageJ software as described previously (Tomatis *et al.*, 2010). For FRAP experiments, cycloheximide was added to the cells 1 h before starting the image acquisition. In the indicated cases, tannic acid, 2-BP, or palmostatin B was also incorporated into the culture medium.

Erk phosphorylation assay

CHO-K1 cells were transfected with H-RasG12V, H-RasG12V(C181S), or H-RasG12V(C184S) or were not transfected as a control, and they incubated overnight in DMEM with 0.5% FBS. Then the cells were left in serum-free DMEM for 3 h at 37°C, and the control cells were stimulated with 10% FBS in DMEM for 15 min. The samples were processed for Western blot analysis as described earlier.

2-BP treatment

A stock solution of 0.5 M 2-BP (Fluka) was prepared in dimethyl sulfoxide (DMSO). To analyze the effect of 2-BP on the steady-state subcellular distribution and membrane-binding properties of H-Ras and its acylation mutants by live-cell imaging experiments, 60 μg/ml cycloheximide was incorporated into the culture medium during transfection. Then, 5 h after transfection, 10% FBS was added to the medium, and 3 h later, 50 μM 2-BP was also incorporated. After 30 min of 2-BP treatment, the cycloheximide was removed. Finally, after 8 h of cycloheximide withdrawal, cells were used in live-cell imaging.

FRET experiments and analysis

CHO-K1 cells were seeded onto 35-mm dishes containing a coverslip and grown to 70–80% confluence at the time of transfection, which was performed as indicated. Then cells were washed with PBS and fixed with 1% paraformaldehyde, and these fixed cells were washed with PBS and rinsed with Milli-Q water. Coverslips were visualized using an Olympus FV300 confocal laser scanning microscope. A Plan Apochromat 60×/1.42 NA oil immersion objective lens was used with digitally zoomed 3×, 512 × 512 image resolution. The ECFP (donor) and EYFP (acceptor) chimeric proteins were excited with an argon laser at 458 and 515 nm, respectively, and the emission channel was 465–495 nm for the donor and 530–560 nm for the acceptor. As a positive control, cells transfected with a chimeric CFP fused to YFP was used. Sensitized emission measurement was chosen, with images processed using the PFRET module for the FV10-ASW software of the FV1000 microscope.

FRAP and FLIP experiments

FRAP and FLIP experiments were performed using an Olympus FluoView FV1000 confocal microscope with a 63× UPlanApo oil immersion/1.42 NA (Olympus) objective. For all of these experiments, the pinhole was fully opened in order to minimize changes in fluorescence detection due to *Z*-drift occurring during time-lapse imaging. For the FRAP experiments, photobleaching was performed using 50× digital zoom, 50 scans of a 200 pixel × 200 pixel bleaching ROI (1024 pixel × 1024 pixel resolution), 8 μs/pixel, direct scan, 100% transmission of both 458- and 488-nm laser lines (30 mW), and a 63× UPlanApo oil immersion/1.42 NA objective. Under these conditions, YFP fluorescence after bleaching was <10% of its initial value. Prebleaching and postbleaching images (3 and 90 images, respectively) were obtained every 10 s from a 512 pixel × 512 pixel resolution using the same objective, with these images acquired sequentially in each channel (YFP and Cherry). For FLIP experiments, bleaching of the ROI and full image acquisition was performed every 2 min and obtained using the same acquisition parameters described for prebleaching and postbleaching images in FRAP experiments.

Photoactivation experiments

CHO-K1 cells were cotransfected with H-Ras(C181S) or H-Ras(C184S) fused to PA-GFP (Patterson and Lippincott-Schwartz, 2004) and Golgi marker GalNAc-T-Cherry or ST3GalII-Cherry (Ruggiero *et al.*, 2015) and analyzed by live-cell imaging microscopy. The experiments were performed at 37°C using a live-cell chamber, with temperature and CO_2 (5% air mix) maintained using a controller device (Tokai Hit) on the Olympus FluoView FV1000 confocal microscope, which had a 63×/1.42 NA objective and confocal aperture set at 370 μm (optical slice, 2.3 μm). In the photoactivation of the Golgi experiments, the area to be photoactivated was selected by analyzing the fluorescence of the Golgi markers in the red channel. This ROI was then irradiated at 405 nm with laser intensity set at 1–10% for 5 s. Postactivation images were taken with 488- and 543-nm lasers to acquire green and cherry fluorescence, respectively, every 15 s over 20 min. For the endoplasmic reticulum photoactivation experiments, a small region far from the Golgi signal was selected and irradiated with 405-nm laser intensity set at 1% for 5 s. Images postactivation were taken every 15 s for 90 s. Then the process was repeated seven times. Photobleaching control experiments were performed using PA-GFP empty vector with the same acquisition conditions as described.

Tannic acid treatment

Tannic acid treatment was performed as described (Trenchi *et al.*, 2009), with some modifications. Briefly, transfected cells grown on Lab-Tek chambered coverglass were incubated at 37°C with 1% tannic acid (MP Biomedicals) in PBS (pH 7) for 10 min. Then these cells

were incubated using the described conditions for FRAP experiments with tannic acid maintained in the Lab-Tek coverglass during the experiment. The tannic acid effect was tested by analyzing its effect on Tf internalization.

ACKNOWLEDGMENTS

We thank J. Valdez Taubas (CIQUIBIC, Córdoba, Argentina) for critical reading of the manuscript and comments. Plasmid coding PA-GFP was kindly supplied by E. Ambroggio (CIQUIBIC). Cerulenin was generously supplied by Diego de Mendoza (Instituto de Biología Molecular y Celular de Rosario, Argentina). We thank C. Mas, C. Sampedro, G. Schachner, and S. Deza for excellent technical assistance with microscope techniques and cell cultures. This work was supported in part by grants from the Secretaría de Ciencia y Tecnología, Universidad Nacional de Córdoba, Consejo Nacional de Investigaciones Científicas y Técnicas (CONICET), the Agencia Nacional de Promoción Científica y Tecnológica, Argentina, and the Mizutani Foundation for Glycoscience (Japan). M.P.P. is the recipient of a CONICET fellowship. A.A.V. and J.L.D are career investigators of CONICET.

REFERENCES

Agudo-Ibanez L, Herrero A, Barbacid M, Crespo P (2015). H-ras distribution and signaling in plasma membrane microdomains are regulated by acylation and deacylation events. Mol Cell Biol 35, 1898–1914.

Ahearn IM, Haigis K, Bar-Sagi D, Philips MR (2012). Regulating the regulator: post-translational modification of RAS. Nat Rev Mol Cell Biol 13, 39–51.

Ahearn IM, Tsai FD, Court H, Zhou M, Jennings BC, Ahmed M, Fehrenbacher N, Linder ME, Philips MR (2011). FKBP12 binds to acylated H-ras and promotes depalmitoylation. Mol Cell 41, 173–185.

Arozarena I, Calvo F, Crespo P (2011). Ras, an actor on many stages: post-translational modifications, localization, and site-specified events. Genes Cancer 2, 182–194.

Baines AT, Xu D, Der CJ (2011). Inhibition of Ras for cancer treatment: the search continues. Future Med Chem 3, 1787–1808.

Beronja S, Janki P, Heller E, Lien WH, Keyes BE, Oshimori N, Fuchs E (2013). RNAi screens in mice identify physiological regulators of oncogenic growth. Nature 501, 185–190.

Chamberlain LH, Shipston MJ (2015). The physiology of protein S-acylation. Physiol Rev 95, 341–376.

Chen HQ, Tannous M, Veluthakal R, Amin R, Kowluru A (2003). Novel roles for palmitoylation of Ras in IL-1 beta-induced nitric oxide release and caspase 3 activation in insulin-secreting beta cells. Biochem Pharmacol 66, 1681–1694.

Chiu VK, Bivona T, Hach A, Sajous JB, Silletti J, Wiener H, Johnson RL 2nd, Cox AD, Philips MR (2002). Ras signalling on the endoplasmic reticulum and the Golgi. Nat Cell Biol 4, 343–350.

Choy E, Chiu VK, Silletti J, Feoktistov M, Morimoto T, Michaelson D, Ivanov IE, Philips MR (1999). Endomembrane trafficking of ras: the CAAX motif targets proteins to the ER and Golgi. Cell 98, 69–80.

Christner C, Wyrwa R, Marsch S, Kullertz G, Thiericke R, Grabley S, Schumann D, Fischer G (1999). Synthesis and cytotoxic evaluation of cycloheximide derivatives as potential inhibitors of FKBP12 with neuroregenerative properties. J Med Chem 42, 3615–3622.

Cox AD, Der CJ, Philips MR (2015). Targeting RAS membrane association: back to the future for Anti-RAS drug discovery? Clin Cancer Res 21, 1819–1827.

Crespo PM, Zurita AR, Daniotti JL (2002). Effect of gangliosides on the distribution of a glycosylphosphatidylinositol-anchored protein in plasma membrane from Chinese hamster ovary-K1 cells. J Biol Chem 277, 44731–44739.

Dallavilla T, Abrami L, Sandoz PA, Savoglidis G, Hatzimanikatis V, van der Goot FG (2016). Model-driven understanding of palmitoylation dynamics: Regulated acylation of the endoplasmic reticulum chaperone calnexin. PLoS Comput Biol 12, e1004774.

Dekker FJ, Rocks O, Vartak N, Menninger S, Hedberg C, Balamurugan R, Wetzel S, Renner S, Gerauer M, Scholermann B, *et al.* (2010). Small-molecule inhibition of APT1 affects Ras localization and signaling. Nat Chem Biol 6, 449–456.

Di Fiore PP, Gill GN (1999). Endocytosis and mitogenic signaling. Curr Opin Cell Biol 11, 483–488.

Duncan JA, Gilman AG (1998). A cytoplasmic acyl-protein thioesterase that removes palmitate from G protein alpha subunits and p21(RAS). J Biol Chem 273, 15830–15837.

Eisenberg S, Laude AJ, Beckett AJ, Mageean CJ, Aran V, Hernandez-Valladares M, Henis YI, Prior IA (2013). The role of palmitoylation in regulating Ras localization and function. Biochem Soc Trans 41, 79–83.

Giraudo CG, Rosales Fritz VM, Maccioni HJ (1999). GA2/GM2/GD2 synthase localizes to the trans-golgi network of CHO-K1 cells. Biochem J 342, 633–640.

Gomez GA, Daniotti JL (2005). H-Ras dynamically interacts with recycling endosomes in CHO-K1 cells: involvement of Rab5 and Rab11 in the trafficking of H-Ras to this pericentriolar endocytic compartment. J Biol Chem 280, 34997–35010.

Gomez GA, Daniotti JL (2007). Electrical properties of plasma membrane modulate subcellular distribution of K-Ras. FEBS J 274, 2210–2228.

Goodwin JS, Drake KR, Rogers C, Wright L, Lippincott-Schwartz J, Philips MR, Kenworthy AK (2005). Depalmitoylated Ras traffics to and from the Golgi complex via a nonvesicular pathway. J Cell Biol 170, 261–272.

Gorfe AA, McCammon JA (2008). Similar membrane affinity of mono- and di-S-acylated ras membrane anchors: a new twist in the role of protein lipidation. J Am Chem Soc 130, 12624–12625.

Hancock JF (2003). Ras proteins: different signals from different locations. Nat Rev Mol Cell Biol 4, 373–384.

Hedberg C, Dekker FJ, Rusch M, Renner S, Wetzel S, Vartak N, Gerding-Reimers C, Bon RS, Bastiaens PI, Waldmann H (2011). Development of highly potent inhibitors of the Ras-targeting human acyl protein thioesterases based on substrate similarity design. Angew Chem Int Ed Engl 50, 9832–9837.

Hobbs GA, Der CJ, Rossman KL (2016). RAS isoforms and mutations in cancer at a glance. J Cell Sci 129, 1287–1292.

Iglesias-Bartolome R, Crespo PM, Gomez GA, Daniotti JL (2006). The antibody to GD3 ganglioside, R24, is rapidly endocytosed and recycled to the plasma membrane via the endocytic recycling compartment. Inhibitory effect of brefeldin A and monensin. FEBS J 273, 1744–1758.

Jiang X, Sorkin A (2002). Coordinated traffic of Grb2 and Ras during epidermal growth factor receptor endocytosis visualized in living cells. Mol Biol Cell 13, 1522–1535.

Kanaani J, Patterson G, Schaufele F, Lippincott-Schwartz J, Baekkeskov S (2008). A palmitoylation cycle dynamically regulates partitioning of the GABA-synthesizing enzyme GAD65 between ER-Golgi and post-Golgi membranes. J Cell Sci 121, 437–449.

Lawrence DS, Zilfou JT, Smith CD (1999). Structure-activity studies of cerulenin analogues as protein palmitoylation inhibitors. J Med Chem 42, 4932–4941.

Liang X, Lu Y, Neubert TA, Resh MD (2002). Mass spectrometric analysis of GAP-43/neuromodulin reveals the presence of a variety of fatty acylated species. J Biol Chem 277, 33032–33040.

Lin DT, Conibear E (2015a). ABHD17 proteins are novel protein depalmitoylases that regulate N-Ras palmitate turnover and subcellular localization. Elife 4, e11306.

Lin DT, Conibear E (2015b). Enzymatic protein depalmitoylation by acyl protein thioesterases. Biochem Soc Trans 43, 193–198.

Lobo S, Greentree WK, Linder ME, Deschenes RJ (2002). Identification of a Ras palmitoyltransferase in Saccharomyces cerevisiae. J Biol Chem 277, 41268–41273.

Paladino S, Pocard T, Catino MA, Zurzolo C (2006). GPI-anchored proteins are directly targeted to the apical surface in fully polarized MDCK cells. J Cell Biol 172, 1023–1034.

Patterson GH, Lippincott-Schwartz J (2004). Selective photolabeling of proteins using photoactivatable GFP. Methods 32, 445–450.

Pedro MP, Vilcaes AA, Tomatis VM, Oliveira RG, Gomez GA, Daniotti JL (2013). 2-Bromopalmitate reduces protein deacylation by inhibition of acyl-protein thioesterase enzymatic activities. PLoS One 8, e75232.

Pol A, Calvo M, Enrich C (1998). Isolated endosomes from quiescent rat liver contain the signal transduction machinery. Differential distribution of activated Raf-1 and Mek in the endocytic compartment. FEBS Lett 441, 34–38.

Polishchuk R, Di Pentima A, Lippincott-Schwartz J (2004). Delivery of raft-associated, GPI-anchored proteins to the apical surface of polarized MDCK cells by a transcytotic pathway. Nat Cell Biol 6, 297–307.

Rizzo MA, Kraft CA, Watkins SC, Levitan ES, Romero G (2001). Agonist-dependent traffic of raft-associated Ras and Raf-1 is required for activation of the mitogen-activated protein kinase cascade. J Biol Chem 276, 34928–34933.

Rizzo MA, Shome K, Watkins SC, Romero G (2000). The recruitment of Raf-1 to membranes is mediated by direct interaction with phosphatidic acid and is independent of association with Ras. J Biol Chem 275, 23911–23918.
Rocks O, Gerauer M, Vartak N, Koch S, Huang ZP, Pechlivanis M, Kuhlmann J, Brunsveld L, Chandra A, Ellinger B, *et al*. (2010). The palmitoylation machinery is a spatially organizing system for peripheral membrane proteins. Cell 141, 458–471.
Rocks O, Peyker A, Kahms M, Verveer PJ, Koerner C, Lumbierres M, Kuhlmann J, Waldmann H, Wittinghofer A, Bastiaens PI (2005). An acylation cycle regulates localization and activity of palmitoylated Ras isoforms. Science 307, 1746–1752.
Roy S, Plowman S, Rotblat B, Prior IA, Muncke C, Grainger S, Parton RG, Henis YI, Kloog Y, Hancock JF (2005). Individual palmitoyl residues serve distinct roles in H-ras trafficking, microlocalization, and signaling. Mol Cell Biol 25, 6722–6733.
Ruggiero FM, Vilcaes AA, Iglesias-Bartolome R, Daniotti JL (2015). Critical role of evolutionarily conserved glycosylation at Asn211 in the intracellular trafficking and activity of sialyltransferase ST3Gal-II. Biochem J 469, 83–95.
Rusch M, Zimmermann TJ, Burger M, Dekker FJ, Gormer K, Triola G, Brockmeyer A, Janning P, Bottcher T, Sieber SA, *et al*. (2011). Identification of acyl protein thioesterases 1 and 2 as the cellular targets of the Ras-signaling modulators palmostatin B and M. Angew Chem Int Ed Engl 50, 9838–9842.
Salaun C, Greaves J, Chamberlain LH (2010). The intracellular dynamic of protein palmitoylation. J Cell Biol 191, 1229–1238.
Silvius JR, Bhagatji P, Leventis R, Terrone D (2006). K-ras4B and prenylated proteins lacking "second signals" associate dynamically with cellular membranes. Mol Biol Cell 17, 192–202.
Spiegel J, Cromm PM, Zimmermann G, Grossmann TN, Waldmann H (2014). Small-molecule modulation of Ras signaling. Nat Chem Biol 10, 613–622.
Swarthout JT, Lobo S, Farh L, Croke MR, Greentree WK, Deschenes RJ, Linder ME (2005). DHHC9 and GCP16 constitute a human protein fatty acyltransferase with specificity for H- and N-Ras. J Biol Chem 280, 31141–31148.
Tomatis VM, Trenchi A, Gomez GA, Daniotti JL (2010). Acyl-protein thioesterase 2 catalyzes the deacylation of peripheral membrane-associated GAP-43. PLoS One 5, e15045.
Trenchi A, Gomez GA, Daniotti JL (2009). Dual acylation is required for trafficking of growth-associated protein-43 (GAP-43) to endosomal recycling compartment via an Arf6-associated endocytic vesicular pathway. Biochem J 421, 357–369.
Verstraeten VL, Peckham LA, Olive M, Capell BC, Collins FS, Nabel EG, Young SG, Fong LG, Lammerding J (2011). Protein farnesylation inhibitors cause donut-shaped cell nuclei attributable to a centrosome separation defect. Proc Natl Acad Sci USA 108, 4997–5002.
Wan J, Roth AF, Bailey AO, Davis NG (2007). Palmitoylated proteins: purification and identification. Nat Protoc 2, 1573–1584.
Wennerberg K, Rossman KL, Der CJ (2005). The Ras superfamily at a glance. J Cell Sci 118, 843–846.
Wright LP, Philips MR (2006). Thematic review series: Lipid posttranslational modifications. CAAX modification and membrane targeting of Ras. J Lipid Res 47, 883–891.
Xu J, Hedberg C, Dekker FJ, Li Q, Haigis KM, Hwang E, Waldmann H, Shannon K (2012). Inhibiting the palmitoylation/depalmitoylation cycle selectively reduces the growth of hematopoietic cells expressing oncogenic Nras. Blood 119, 1032–1035.
Yokoi N, Fukata Y, Sekiya A, Murakami T, Kobayashi K, Fukata M (2016). Identification of PSD-95 depalmitoylating enzymes. J Neurosci 36, 6431–6444.
Zeidman R, Jackson CS, Magee AI (2009). Protein acyl thioesterases (Review). Mol Membr Biol 26, 32–41.